Journal of Power Sources 228 (2013) 24–31

Contents lists available at SciVerse ScienceDirect

Journal of Power Sources

journal homepage: www.elsevier.com/locate/jpowsour

Mass transport and electrolyte accessibility through hexagonally ordered channels of self-assembled mesoporous carbons

Shunsuke Tanaka [a,b,*], Anna Doi [a], Takatomo Matsui [a], Yoshikazu Miyake [a,b]

[a] Department of Chemical, Energy and Environmental Engineering, Faculty of Environmental and Urban Engineering, Kansai University, 3-3-35 Yamate-cho, Suita-shi, Osaka 564-8680, Japan
[b] High Technology Research Center, Kansai University, 3-3-35 Yamate-cho, Suita-shi, Osaka 564-8680, Japan

HIGHLIGHTS

- Hexagonal *p6mm* symmetry was used as a model structure to understand EDLC behavior.
- The lengthy straight channels act as ion-highways and allow for fast ion transport.
- The micropores connecting mesochannels dramatically slow down the ion transport.
- The mesochannel length can be dominant factor determining the ion transport.

ARTICLE INFO

Article history:
Received 6 September 2012
Received in revised form
31 October 2012
Accepted 27 November 2012
Available online 2 December 2012

Keywords:
Ordered mesoporous carbons
Straight mesochannels
Pore tortuosity
Capacitive performance
Mass transport
Pore accessibility

ABSTRACT

Ordered mesoporous carbons have attracted great interest for their potential use to electrodes for electric double layer capacitors. However, it is crucial to develop an electrode such that the active sites within the mesoporous carbons are accessible to electrolyte solution species via facile mass transport through well-defined pores. Here, we investigate the electrolyte accessibility and the effective mass transport for the ordered mesoporous carbons possessing *p6mm* symmetry, whereas having different mesochannel length, formed by soft-templating self-assembly. Mesoporous carbons were prepared from a thermosetting phenolic resin and a thermally decomposable copolymer template in ethanol/water solutions of different molar ratios. The general evolution of the mesophase follows the trends that are expected based on packing parameters due to swelling of the hydrophobic volume of the copolymer micelles. However, changes in mesochannel length and the degree of long-range order are found to depend on ethanol/water ratio. Electrochemical impedance spectroscopy was used to assess the transport properties. The impedance data clearly demonstrated that the degree of long-range order and channel length can be a dominant factor that determines the transport and the degree to which the equilibrium adsorption sites are accessible. The lengthy mesochannels in well-ordered mesoporous carbon serve as ion-highways and allow for very fast mass transport into the micropores of the channel frameworks.

1. Introduction

Ordered mesoporous materials formed via self-assembly of surfactants and framework sources are unique because they possess regular arrays of uniform channels [1–6]. Ordered mesoporous carbons were initially made by hard-templating method using silica templates [7–10] but were later synthesized by soft-templating method using thermally decomposable triblock copolymers [11–16]. This method uses the organic–organic interaction between a thermosetting polymer resin and copolymer to form an ordered nanocomposite by self-assembly. The thermosetting polymer resin is carbonized by heating under inert atmosphere, after which process it remains as a carbon pore walls containing micropores. On the other hand, the surfactant can be burned out to form uniform mesopores. The advantages of this method are to be able to perform large-quantity synthesis and easy morphology control, and to obtain ordered mesoporous straight channels which have never before been seen in mesoporous carbons obtained by the hard-templating method. Thus, the obtained mesoporous carbons are fascinating for model material for host-guest applications.

Such mesoporous carbons have potential applications as adsorbents, sensors, catalyst supports, membrane separations,

* Corresponding author. Department of Chemical, Energy and Environmental Engineering, Faculty of Environmental and Urban Engineering, Kansai University, 3-3-35 Yamate-cho, Suita-shi, Osaka 564-8680, Japan. Tel.: +81 6 6368 0851; fax: +81 6 6388 8869.
E-mail address: shun_tnk@kansai-u.ac.jp (S. Tanaka).

0378-7753/$ – see front matter © 2012 Elsevier B.V. All rights reserved.
http://dx.doi.org/10.1016/j.jpowsour.2012.11.114

hosts for biomaterials, templates for nanoparticles, and electric devices, and energy storage and conversion systems [17–19]. The development of advanced electric double layer capacitors (EDLC) which are electrical storage media based on the physisorption of ions and improvement in the understanding of the transport and adsorption phenomena of electrolyte ions within carbon media has attracted much attention [20–22]. In theory, the capacitance of EDLC should be proportional to the specific surface area of carbon media. However, many studies have shown an unfavorable divergence from this linear relation. The performance of EDLC depends on the properties of the carbon media, such as pore size, pore structure, surface functional groups, and electronic conductivity [23–37]. However, it is difficult to draw a simple relationship between the structural and morphological properties of carbon media and the EDLC performance, because of the complicated structures of the carbon media. Many researchers have therefore made great efforts to reveal the mechanism of EDLC by using accurate designed carbon materials as model electrodes. Simon's group has reported the critical effect of the pore size on the capacitance by using carbide-derived carbons with tunable micropore size distributions [28–31]. By using zeolite-templated carbons with ordered micropore structures, Kyotani's group examined the effect of micropore structure on the performance of EDLC [32,33]. Many groups have studied the impacts of the ordered mesopores on ion transport by evaluating the rate performance of EDLC which are based on ordered mesoporous carbons prepared by the hard-templating method [34–36]. Long's group has recently reported the effects of mesopore symmetry on the ion transport by using mesoporous carbons with three-dimensional cubic, two-dimensional hexagonal, and wormhole-like mesostructures formed by the soft-templating self-assembly [37]. The use of such accurate designed model materials is thus useful towards understanding the mechanism of EDLC.

The specific capacitance and energy storage characteristics of EDLC are strongly affected by the capability of carbon media to adsorb a large quantity of ions under an applied potential and attract the ions closer to the pore walls. The capacitive rate performance is determined by how fast the ions can travel within the pores. Introducing the mesoporous structure has been proved effective for increasing the capacitance. However, it is not the mesopore surfaces but micropore surfaces that mainly store ions from a viewpoint of surface area contribution. Besides the mesopore size and arrangement, the pore depth, tortuosity, and accessibility must be useful for transport behavior, limiting the sizes and orientations of solvated ions. In this report we focus on how differences in the mesochannel length and the degree of long-range order influence the EDLC performance, especially the mass transport resistance, electrolyte accessibility, charging kinetics, and frequency responses, and aim to contribute to the design of advanced mesoporous carbons and open a new strategy towards preparation of the electrode carbon materials.

2. Experimental

2.1. Chemicals

Resorcinol, phloroglucinol, formaldehyde (36–38 wt%), 5 N HCl, and ethanol were purchased from Wako Pure Chemical Industries and used as received. Pluronic F127 was purchased from Sigma–Aldrich Chemical Co. and used as received.

2.2. Soft-templating synthesis of ordered mesoporous carbons

Resorcinol and phloroglucinol were completely dissolved in ethanol/water solution, HCl was added, and the solution was stirred for 30 min. Pluronic F127 was then added, and after it was completely dissolved, formaldehyde was added. The final molar composition of the coating solution was 3 resorcinol: 1 phloroglucinol: 0.02 Pluronic F127: 9 formaldehyde: 0.1 HCl: 20–200 ethanol: 40 water. The solutions were left at room temperature over night, during which they separated into two phases. The upper clear phase was discarded; the lower dark brown phases were preheated at 100 °C for 1 h in air. The resultant brown deposition was carbonized under a nitrogen atmosphere at 800 or 1000 °C for 3 h at a heating rate of 1 °C min^{-1}.

2.3. Characterization

The ordered structure of the samples was investigated with small-angle X-ray scattering (SAXS). SAXS measurements were recorded on an MXP-SAXS3 MO3XHF (Mac Science Co., Ltd.) using Cu Kα radiation with $\lambda = 1.5418$ Å; the copper anode was operated at 40 kV and 30 mA. Nitrogen adsorption/desorption isotherms of the samples were measured at 77 K using a BELSORP-max instrument (Bel Japan, Inc.), and the surface area was determined using the Brunauer–Emmett–Teller (BET) formalism. The pore size distribution was derived from the adsorption branches of the isotherms by the Barrett–Joyner–Halenda (BJH) model. Transmission electron microscopy (TEM) images of the mesoporous carbons were recorded on a JEM-2010 microscope (JEOL Ltd.) at an acceleration voltage of 200 kV.

2.4. Electrochemical measurements

The mesoporous carbons were mixed with polytetrafluoroethylene (PTFE) (Daikin Industries, Ltd.) binder and carbon black to form composites consisting of 80 wt% mesoporous carbon, 10 wt% PTFE, and 10 wt% carbon black. The resulting composite paste was made into a rubbery film of about 0.2 mm in thickness and left to dry under vacuum at 80 °C over night. The film was cut into 1 cm × 1 cm pieces and used as electrodes. Pt plate coated by a thin layer of conductive paint was used as a current collector. The conductive paint was used to reduce the interfacial resistance between the electrode and the current collector. In addition, Pt–electrode–separator–electrode–Pt sandwich was pressed at 1 MPa to reduce the interfacial resistance. The EDLC were assembled in a three-electrode configuration in aqueous 1 M H_2SO_4 and 0.5 M tetraethylammonium tetrafluoroborate (Et_4NBF_4)/polypropylene carbonate (PC) electrolyte solutions. An Ag/AgCl was used as a reference electrode. The electrodes were then exposed to a vacuum for 1 h to impregnate an electrolyte solution into the working and counter electrodes. Electrochemical measurements consisted of cyclic voltammetry (CV) and EIS using a charge–discharge apparatus (HX5000, Hokuto Denko). The EIS measurements were carried out in the frequency range of 10 mHz–20 kHz with a 10 mV AC amplitude. All the electrochemical measurements were carried out at 25 °C.

3. Results and discussion

3.1. Synthesis and characterization of ordered mesoporous carbons

Fig. 1 shows SAXS patterns of carbonized powdery samples prepared by the sol–gel method. The ethanol/water molar ratio in the precursor solution ranges from 0.5 to 5.0. For the powder synthesis, the dark brown glue-like precipitates were obtained and pyrolyzed to form powdery solids. The samples look like rocky fragments on the order of several tens of millimeters and can be easily crushed into a fine powder. Since the particle size of mesoporous carbons can affect the inner electrical resistance, the

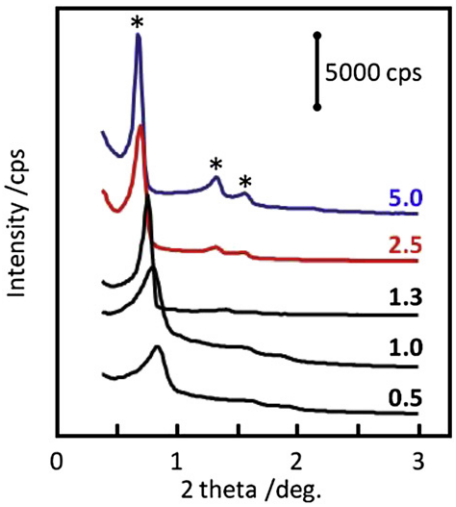

Fig. 1. SAXS patterns of mesoporous carbons prepared at different ethanol/water molar ratios. The carbonization temperature was 800 °C.

particle size was adjusted to be almost the same (75 ± 29 μm) by dry grinding in ceramic ball mill and sieving process. All the SAXS patterns exhibit three peaks in the region of $2\theta = 0.5–2.0°$, which can be indexed as the (100), (110), and (200) reflections associated with the two-dimensional hexagonal *p*6*mm* symmetry. As the ethanol/water molar ratio increased, the well-resolved higher order peaks, (110) and (200) appeared in the SAXS pattern, indicating the development of long-range order of the channel system. At ethanol/water molar ratios ranging from 0.5 to 1.3, the higher order peaks were less sharp, again suggesting an inferior order in the channel structure.

Fig. 2 shows TEM images of mesoporous carbons prepared at ethanol/water molar ratios ranging from 1.0 to 5.0. Three kinds of mesostructures were defined by using SAXS analysis and TEM observations. The mesoporous structure is composed of a short mesochannels interconnected in a wormhole-like at ethanol/water molar ratio of 1.0 and 1.3. The pore structure is similar to silica and carbon films with a wormhole-like structure reported by Tate et al. [38] and Jin et al. [39], respectively. The samples with the short wormlike mesoporous channels are designated short-range order (SRO). At high ethanol/water ratio the hexagonal *p*6*mm* phase with long-range order (LRO) is favored while at moderate ethanol/water ratio the *p*6*mm* phase with medium-range order (MRO) is formed. The mesochannels of LRO range up to at least several micrometers in length while those of MRO are several hundred nanometers in length. Ordered straight channels run with coincidence spacing of about 13 nm, which is in reasonable agreement with the *d*-spacing calculated from the SAXS pattern.

The porous structures of the carbons were investigated by nitrogen adsorption/desorption measurements shown in Fig. 3. At ethanol/water molar ratio of 1.3, the powders carbonized at 800 °C show typical type-IV curves with hysteresis loops and sharp capillary condensation, ascribed to the uniform mesopores inside the carbons. Of particular interest is that the hysteresis patterns

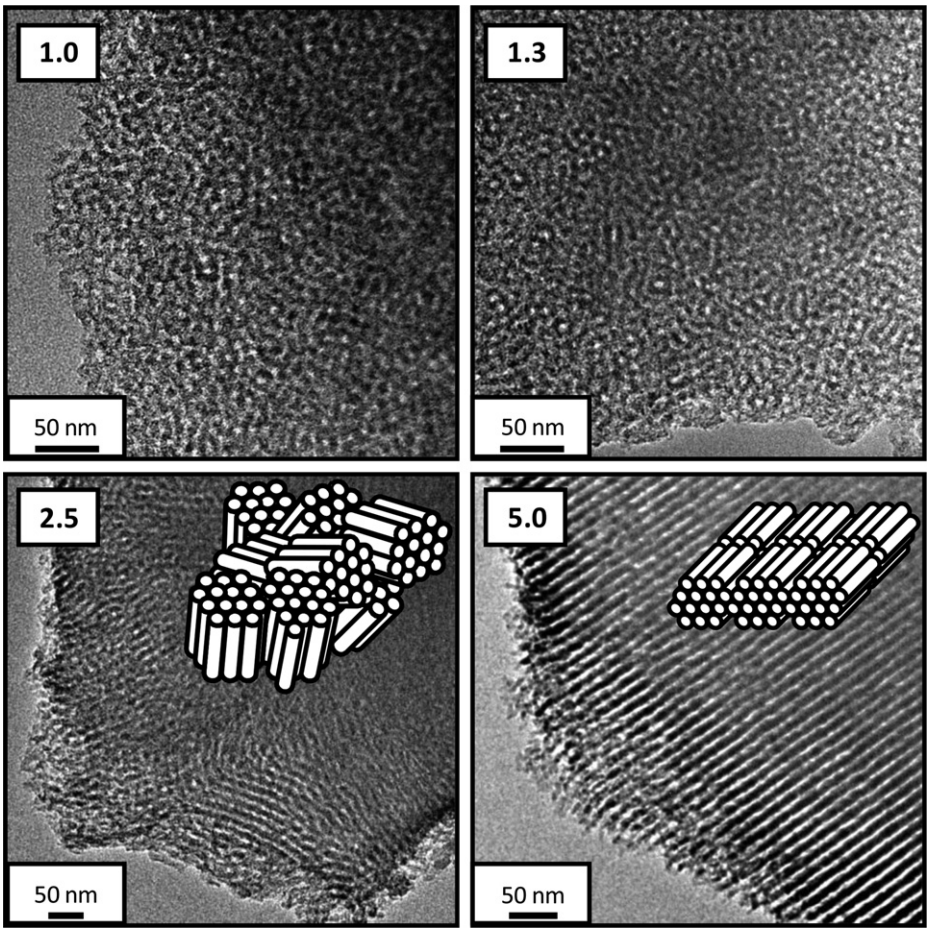

Fig. 2. TEM images of mesoporous carbons prepared at different ethanol/water molar ratios. The carbonization temperature was 800 °C.

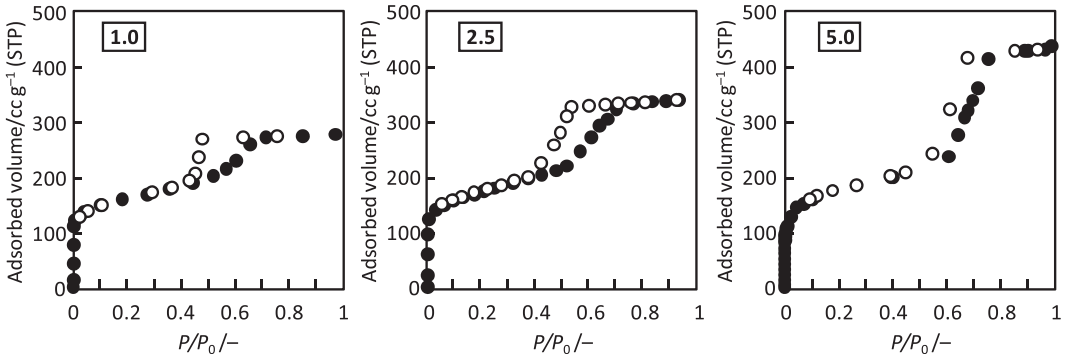

Fig. 3. N_2 adsorption/desorption isotherms of mesoporous carbons prepared at different ethanol/water molar ratios. The carbonization temperature was 800 °C.

differ among the degrees of order, SRO, MRO, and LRO. In adsorption/desorption isotherm of SRO, an asymmetric shape of type-H2 hysteresis loop was observed, which is believed to result from interconnected pore structures [40–44]. The hysteresis loop of LRO was more symmetric shape of type-H1 compared to that of MRO. The type-H1 hysteresis had been associated with porous materials exhibiting a narrow distribution of cylindrical pores open at both ends [44].

3.2. Structures of ordered mesoporous carbons

Table 1 summarizes the results of the pore structure analysis. The *d*-spacing, pore size, pore wall thickness, BET surface area, and pore volume change with ethanol/water molar ratio. Fig. 4 summarizes the variation in the *d*-spacing, pore size, and pore wall thickness as a function of the ethanol/water molar ratio. Both show that the *d*-spacing and pore size slightly increases with increasing ethanol/water molar ratio. On the other hand, there is only a small difference in the pore wall thickness, BET surface area, and micropore volume of the samples at different ethanol/water molar ratios.

The trends in mesophase structure may be rationalized in the context of packing parameters. In this model, the effective area of the headgroup is compared with the volume of the surfactant to control the curvature of micellar array [45]. It takes the form $v/a_0 l_c$ where v is the volume of the hydrophobic segment, a_0 is the effective area of the headgroup, and l_c is the critical chain length. This model predicts spherical aggregates for packing parameters less than 1/3, cylindrical aggregates from 1/3 to 1/2, and lamellar or bicontinuous structures as it increases to 1. For the copolymer systems discussed here, the effective area of the headgroup is difficult to estimate since phenolic resin and solvent associate with the PEO segment. However, the model may be used to understand trends. At higher ethanol/water ratio, the micellar array in which the core is composed of hydrophobic hydrocarbon chains participates in the solubilization of ethanol. The effective area of the headgroup is smaller, tending to favor structures composed of cylindrical aggregates. Incremental addition of ethanol results in a decreasing interfacial curvature together with accompanying increase in pore size. In addition, ethanol swells the hydrophobic volume of the micellar array and interacts with both PPO and PEO segments because it is highly polar molecule. Thus, ethanol is located at the hydrophilic–hydrophobic interface (PEO/PPO) and helps in stabilizing the interface, leading to the formation of lengthy cylindrical aggregates. The well-defined structures follow the expected evolution based on the packing parameter.

From these above results, mesoporous carbons with ordered straight channels of different lengths were found to be obtained. SRO has a lot of mesopore junctions connected with micropores or dense carbon layer. MRO has many domains which are composed of medium-range hexagonal mesostructure exist and oriented with different rotational directions. LRO has exceptional long-range

Table 1
Structural and electrochemical characteristics of mesoporous carbons prepared at different ethanol/water molar ratios. The carbonization temperature was 800 °C.[a]

Ethanol/water	Degree of order	d[b] (nm)	Mesopore size[c] (nm)	Mesopore wall[d] (nm)	S_{BET}[e] (m^2/g)	V_T[f] (cc/g)	V_{micro}[g] (cc/g)	V_{meso}[h] (cc/g)	C_{aq}[i] (F/g)	Cs_{aq}[j] (μF/cm^2)	C_o[k] (F/g)	Cs_o[l] (μF/cm^2)
0.5	SRO	10.6 (–)	4.0 (4.0)	8.2 (–)	490 (410)	0.24 (0.26)	0.20 (0.21)	0.04 (0.05)	68 (59)	14 (14)	8 (–)	2 (–)
1.0	SRO	11.4 (9.7)	5.0 (4.2)	8.2 (7.0)	520 (400)	0.34 (0.24)	0.22 (0.20)	0.12 (0.04)	72 (65)	14 (16)	9 (16)	2 (4)
1.3	SRO	11.8 (10.0)	5.2 (4.4)	8.4 (7.1)	510 (480)	0.36 (0.31)	0.21 (0.20)	0.15 (0.11)	81 (80)	16 (17)	14 (40)	3 (8)
2.5	MRO	12.3 (11.7)	5.7 (5.6)	8.5 (7.9)	640 (510)	0.57 (0.55)	0.24 (0.22)	0.33 (0.33)	153 (128)	24 (25)	69 (86)	11 (17)
5.0	LRO	12.6 (12.4)	6.1 (6.1)	8.4 (8.2)	550 (540)	0.55 (0.55)	0.22 (0.22)	0.33 (0.33)	138 (146)	25 (27)	94 (98)	17 (18)

[a] Values shown in parenthesis are those of carbons carbonized at 1000 °C.
[b] *d*-Spacing calculated from SAXS and Fourier diffractogram of TEM.
[c] Mesopore diameter calculated by the BJH method using adsorption branches.
[d] Mesopore wall thickness calculated by subtracting the pore size from the distance between pores. Distance between pores calculated by the formula $2d/\sqrt{3}$ assuming a hexagonal unit cell.
[e] BET surface area.
[f] Total pore volume calculated as the amount of nitrogen adsorbed at a relative pressure of 0.95.
[g] Micropore volume calculated from the *V*–*t* plot method using the de Boer equation, $t/\text{Å} = \sqrt{[13.99/(\log(P_0/P) + 0.0340)]}$; $V_{micro} = 0.001547Y$, where Y represents the *Y*-intercept in the *V*–*t* plot.
[h] Mesopore volume calculated by subtracting the value of V_{micro} from that of V_T.
[i] Specific capacitance of electrode in 1 M H_2SO_4 electrolyte (potential scan rate is 1 mV s^{-1}); $C_{aq} = \Delta I/2V \cdot m$, where I, V, and m represent the current, the scan rate, and the mass of the carbon sample, respectively.
[j] Interfacial capacitance of electrode in 1 M H_2SO_4 electrolyte (potential scan rate is 1 mV s^{-1}); $Cs_{aq} = C_{aq}/S_{BET}$.
[k] Specific capacitance of electrode in 0.5 M Et_4NBF_4 electrolyte (potential scan rate is 10 mV s^{-1}); C_o calculated as is the case with C_{aq}.
[l] Interfacial capacitance of electrode in 0.5 M Et_4NBF_4 electrolyte (potential scan rate is 10 mV s^{-1}); $Cs_o = C_o/S_{BET}$.

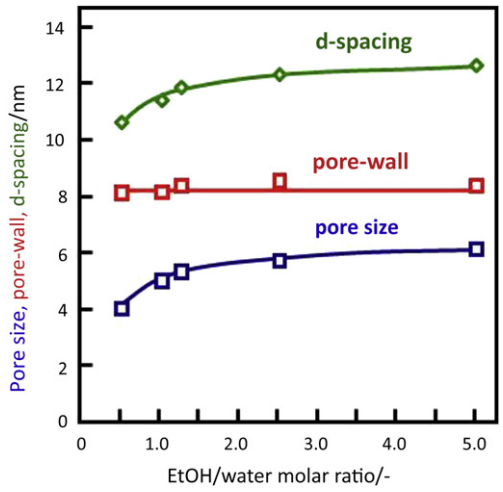

Fig. 4. Variation in the *d*-spacing, pore size, and pore wall thickness as a function of the ethanol/water molar ratio. The carbonization temperature was 800 °C.

hexagonal order with well-organized mesochannels that extend over micrometer-sized regions with few defects and large pore size with narrow pore-size distributions. However, given these above information, the pore accessibility is still not known exactly for SRO, MRO, and LRO. In order to investigate the electrolyte accessibility and mass transport properties of the carbons and discern the effects of pore topology, tortuosity, and channel length, a kinetically-observation of the ion storage/transfer behavior is required. Accordingly, we adopt these mesoporous carbons to further study the effects of pore structure on the EDLC performance. The effect of mesochannel length would become more apparent if the mesoporous carbons with only difference in the degree of order, SRO, MRO, and LRO, were used as model electrodes. Which one is better accessibility and diffusivity? Let's find out their electrochemical performances.

3.3. Electrochemical performances of mesoporous carbons

The CV curves of initial efforts to estimate the electrochemical performance of electrodes are shown in Fig. 5. The capacitance for SRO, MRO, and LRO was evaluated with a three-electrode cell and calculated for one electrode. The electrodes were prepared by pressing procedure to neglect the collector/electrode contact resistance. It can be seen that the CV curves of MRO and LRO electrodes both exhibit a symmetric rectangular shape without obvious redox peaks, indicating typical EDLC behavior. However, the CV curve of SRO was distorted rectangular shape, suggesting that the proton has a higher mobility than that of the larger size sulfate ion in the inner pores of SRO. Of particular interest is that the interfacial capacitance increased with developing the long-range order although there is no large difference in BET surface area. The MRO and LRO electrodes can achieve the interfacial capacitances of up to 25 μF cm^{-2} (Table 1), which are comparable or even better performance compared to the reported literature [46–50]. The capacitance variation with the potential scan rate is an important issue in high-rate capacitors. Fig. 6 shows the scan rate dependence of the relative capacitance. The capacitance decreased with increasing the potential scan rate. However, the capacitance decrease was less sensitive as the degree of order developed. The LRO electrode resulted in excellent capacitance retention at high scan rate.

As in the use of non-aqueous electrolyte, LRO shows superior capacitance. In addition, the carbonization at higher temperature improved their capacitances. The interfacial capacitance of LRO is two times higher than that of commercial activated carbons (5–8 μF cm^{-2}). The size of Et_4N^+ ions is reported to be about 0.7 nm [51]. Therefore, the diffusivity of the Et_4N^+ ions in micropores seems to be much smaller than that of H^+. For ordered mesoporous carbons, the micropores are present in very thin carbon pore walls of about 8 nm. Although there is no large difference in pore wall thickness, LRO has exceptional narrow distributions of pore wall thickness compared to SRO and MRO. Thus, the diffusion path length in pore walls is very short and uniform, which provide a fast penetration of ions. However, it is still unclear at this stage which factor, electronic or ionic conductivity or both, enhanced the capacitance and high-rate performance.

3.4. Electrochemical impedance spectroscopy of mesoporous carbons

Although the CV method can be utilized to estimate the ion transport behavior, it is still unable to precisely describe the actual electrochemical diffusion process. It is quite important to further investigate the influence of pore length and tortuosity on mass transport based on EIS, which is believed to be a powerful tool for obtaining the dynamic information of ion transport and charge transfer [52–56]. Fig. 7 shows the complex-plane Nyquist plots for SRO, MRO, and LRO electrodes. At the high-medium frequency region, all carbons exhibit a depressed semicircle, then straight lines nearly vertical to the realistic impedance axis when frequency is lower than the knee frequency. An electrode/electrolyte interface can be presented by equivalent circuit involving some electronic elements when it is analyzed by EIS. Typical equivalent circuit for EDLCs is shown in Fig. 7. When the charge transfer resistance R_{ct} and mass transport impedance Z_{mt} are assumed for the electrode, the equivalent circuit involves the series of R_{ct} and Z_{mt}, and the

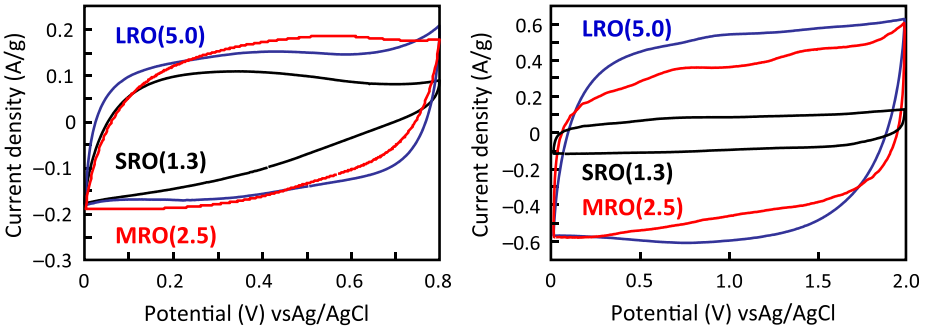

Fig. 5. CV curves of SRO, MRO, and LRO electrodes in 1 M H_2SO_4 electrolyte (left; potential scan rate is 1 mV s^{-1}) and 0.5 M Et_4NBF_4/PC electrolyte (right; potential scan rate is 10 mV s^{-1}). SRO, MRO, and LRO were prepared at ethanol/water molar ratio of 1.3, 2.5, and 5.0, respectively. The carbonization temperature was 800 °C.

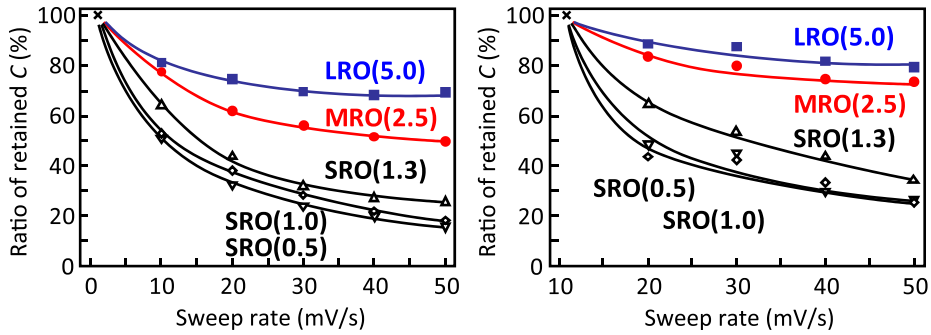

Fig. 6. Capacitance at different potential scan rates for SRO, MRO, and LRO electrodes in 1 M H_2SO_4 electrolyte (left) and 0.5 M Et_4NBF_4/PC electrolyte (right). The mesoporous carbons prepared at different ethanol/water molar ratios. The carbonization temperature was 800 °C.

series element is connected in parallel with the electric double layer capacitance C_{dl}. In addition, they are connected in series with the solution resistance R_{sol}. At high frequency, the impedance can be simplified as follows [53].

$$(\mathrm{Re}(Z) - R_{sol} - R_{ct}/2)^2 + \mathrm{Im}(Z)^2 = (R_{ct}/2)^2$$

The intercept of the curve with the real axis gives an estimation of R_{sol}. In addition, this means that the semicircle diameter is R_{ct}. The semicircle does not depend on C_{dl}. In this case, we used R_{sol} to represent the migration of electrolyte ions in the bulk solution. Thus, it is nearly constant with the same electrolyte condition. Z_{mt} is used to represent the ion diffusion within the mesoporous carbons. R_{ct} includes the bulk carbon, grain boundary, and interface resistances. The interfaces are at the electrode/collector and at the electrolyte/pore surface of mesoporous carbons. There is no large difference in the bulk carbon and electrode/collector interface resistances. Then, R_{ct} depends on the interface resistance at the electrolyte/pore surface of mesoporous carbons. The semicircle diameter reflects R_{ct} which is strongly dependent on the area of contact between the mesopore surface of carbons and electrolyte solution, and electron conduction abilities can be used to estimate the formation rate of the double layer. Note that the present EDLC system is free from the Faradaic processes. As revealed by the semicircle, R_{ct} decreased with increasing the degree of order and increasing carbonization temperature, in good agreement with CV results. It depends on the interface resistance at electrolyte/pore surface of mesoporous carbons due to the electrolyte wettability. At lower frequency, all electrodes exhibit the straight line which is the capacitive behavior. The deviation from the vertical line is attributable to inner-mesopore diffusion resistance Z_{mt} for electrolyte ions. The advantage of using impedance is that it can separate these elementary steps. It can be concluded that the LRO electrode is more favorable for fast ion transport and charge transfer, while the SRO electrode shows the lower capacitive performance.

EIS allowed us to estimate the capacitance changes with the operating frequency. The change in absolute value of impedance and capacitance with operating frequency can be estimated based on EIS, as shown in Fig. 8. The electrolyte ions start to diffuse into the mesopores and then into micropores with decreasing frequency. Thus, the absolute value of impedance and capacitance increased with decreasing frequency. On the other hand, the capacitance remains almost constant at the lower frequencies. The ac-signal can reach and charge more of the inner surface sites of the carbon electrode with decreasing frequency [55,56]. The capacitance of SRO electrode was not saturated even at 0.01 Hz. SRO has a lot of mesopore junctions connected with micropores or dense carbon layer. Thus, the narrow bottle-necks prevent the achieving the equilibrium ion adsorption within 100 s time period. On the other hand, most of the electrolyte ions can reach the adsorption sites in bulk of LRO and MRO mesoporous carbons. This indicates that the ac-signal penetrates the inner surface sites of LRO electrode more deeply than MRO and SRO electrodes, resulting in a higher capacitance. This was attributed to the fact that the ac-

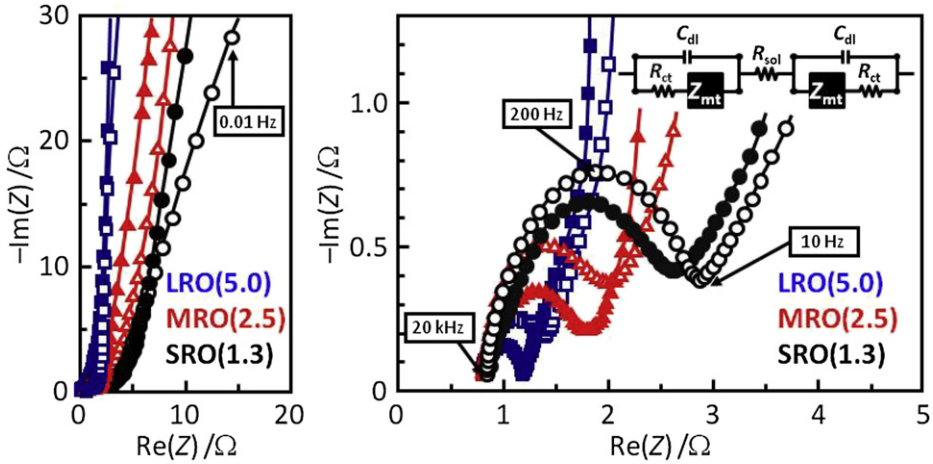

Fig. 7. Complex-plane Nyquist plots in the frequency ranging from 10 mHz to 20 kHz for SRO, MRO, and LRO electrodes in 0.5 M Et_4NBF_4/PC electrolyte. SRO, MRO, and LRO were prepared at ethanol/water molar ratio of 1.3, 2.5, and 5.0, respectively. The carbonization temperature was 800 (open symbols) and 1000 °C (closed symbols). The right figure is magnified view of left figure at higher frequencies.

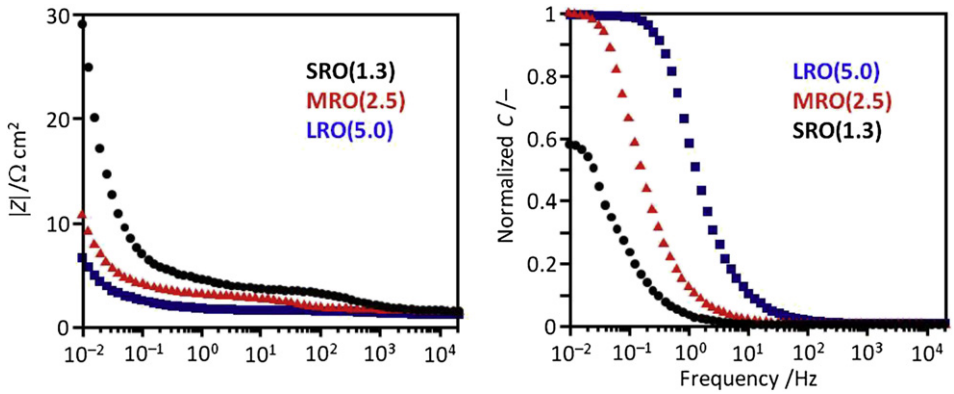

Fig. 8. Change in absolute value of impedance (upper) and capacitance (bottom) with operating frequency for SRO, MRO, and LRO electrodes in 0.5 M Et_4NBF_4/PC electrolyte. SRO, MRO, and LRO were prepared at ethanol/water molar ratio of 1.3, 2.5, and 5.0, respectively. The carbonization temperature was 1000 °C.

signal was able to charge more inner surface sites because the wetted surface area of electrode increased due to the mesopore accessibility. We note that the specific surface area is dominated by micropores, suggesting that it is important to understand how utilize the micropore surface using mesopore highways. The EIS demonstrated that the LRO electrode has superior mass transport ability due to low pore tortuosity. The wettability with electrolyte improved with increasing the degree of long-range order and developing the narrow distribution of pore wall thickness.

4. Conclusions

We have presented a simple and straightforward method for the preparation of ordered mesoporous carbons with straight channels. The hexagonal mesochannels grow in length by adjusting the ethanol/water molar ratio in the precursor solution. Here we present the systematic investigations of the ion storage/transport behavior in EDLC by using highly ordered and well-characterized mesoporous carbons as model electrodes. It was found that the degree of order and pore tortuosity can be dominant factor that determines the ion transport and wettability with electrolyte. The ordered straight channels act as ion-highways, leading to an excellent frequency response and outstanding capacitance retention. EIS demonstrated that for SRO and MRO mesoporous carbons, the interconnected micropores and narrow bottle-necks of mesopores dramatically slow down the ion transport. For LRO mesoporous carbon, the lengthy cylindrical mesostructure facilitates the faster ion transport along their straight mesochannels than within tortuous pathway of SRO and MRO mesopores. The preparation and application of long-range ordered mesoporous carbon overcame the limitations of slow intraparticle ion transport and showed a route for further EDLC performance enhancement.

Acknowledgment

We are grateful for financial support from the Murata Science Foundation, Nippon Sheet Glass Foundation for Materials Science and Engineering, and the A-STEP FS Stage of the Japan Science and Technology Agency (JST).

References

[1] T. Yanagisawa, T. Shimizu, K. Kuroda, C. Kato, Bulletin of the Chemical Society of Japan 63 (1990) 988–992.
[2] S. Inagaki, A. Koiwai, N. Suzuki, Y. Fukushima, K. Kuroda, Bulletin of the Chemical Society of Japan 69 (1996) 1449–1457.
[3] C.T. Kresge, M.E. Leonowicz, W.J. Roth, J.C. Vartuli, J.S. Beck, Nature 359 (1992) 710–712.
[4] J.S. Beck, J.C. Vartuli, W.J. Roth, M.E. Leonowicz, C.T. Kresge, K.D. Schmitt, C.T.W. Chu, D.H. Olson, E.W. Sheppard, S.B. Mccullen, J.B. Higgins, J.L. Schlenker, Journal of American Chemical Society 114 (1992) 10,834–10,843.
[5] Q.S. Huo, D.I. Margolese, U. Ciesla, P.Y. Feng, T.E. Gier, P. Sieger, R. Leon, P.M. Petroff, F. Schuth, G.D. Stucky, Nature 368 (1994) 317–321.
[6] A. Firouzi, D. Kumar, L.M. Bull, T. Besier, P. Sieger, Q. Huo, S.A. Walker, J.A. Zasadzinski, C. Glinka, J. Nicol, D. Margolese, G.D. Stucky, B.F. Chmelka, Science 267 (1995) 1138–1143.
[7] J. Lee, S. Yoon, T. Hyeon, S.M. Oh, K.B. Kim, Chemical Communications (1999) 2177–2178.
[8] R. Ryoo, S.H. Joo, S. Jun, Journal of Physical Chemistry B 103 (1999) 7743–7746.
[9] R. Ryoo, S.H. Joo, M. Kruk, M. Jaroniec, Advanced Materials 13 (2001) 677–681.
[10] J.S. Lee, S.H. Joo, R. Ryoo, Journal of American Chemical Society 124 (2002) 1156–1157.
[11] S. Tanaka, N. Nishiyama, Y. Egashira, K. Ueyama, Chemical Communications (2005) 2125–2127.
[12] S. Tanaka, Y. Katayama, M.P. Tate, H.W. Hillhouse, Y. Miyake, Journal of Materials Chemistry 17 (2007) 3639–3645.
[13] S. Tanaka, A. Doi, N. Nakatani, Y. Katayama, Y. Miyake, Carbon 47 (2009) 2688–2698.
[14] Y. Meng, D. Gu, F.Q. Zhang, Y.F. Shi, H.F. Yang, Z. Li, C.Z. Yu, B. Tu, D.Y. Zhao, Angewandte Chemie International Edition 44 (2005) 7053–7059.
[15] F.Q. Zhang, Y. Meng, D. Gu, Y. Yan, C.Z. Yu, B. Tu, D.Y. Zhao, Journal of American Chemical Society 127 (2005) 13,508–13,509.
[16] C.D. Liang, S. Dai, Journal of American Chemical Society 128 (2006) 5316–5317.
[17] M.E. Davis, Nature 417 (2002) 813–821.
[18] M. Hartmann, Chemistry of Materials 17 (2005) 4577–4593.
[19] J. Lee, J. Kim, T. Hyeon, Advanced Materials 18 (2006) 2073–2094.
[20] B.E. Conway, Electrochemical Supercapacitors: Scientific Fundamentals and Technological Applications, Kluwer Academic/Plenum Publishers, New York, 1999.
[21] A.S. Aricò, P. Bruce, B. Scrosati, J.M. Tarascon, W. van Schalkwijk, Nature Materials 4 (2005) 366–377.
[22] J.R. Miller, P. Simon, Science 321 (2008) 651–652.
[23] D.Y. Qu, Journal of Power Sources 109 (2002) 403–411.
[24] K. Jurewicz, K. Babel, A. Ziolkowski, H. Wachowska, Electrochimica Acta 48 (2003) 1491–1498.
[25] M. Zuleta, M. Bursell, P. Bjornbom, A. Lundblad, Journal of Electroanalytical Chemistry 549 (2003) 101–108.
[26] M. Zuleta, P. Bjornbom, A. Lundblad, G. Nurk, H. Kasuk, E. Lust, Journal of Electroanalytical Chemistry 586 (2006) 247–259.
[27] E. Raymundo-Pinero, K. Kierzek, J. Machnikowski, F. Beguin, Carbon 44 (2006) 2498–2507.
[28] P. Simon, Y. Gogotsi, Nature Materials 7 (2008) 845–854.
[29] J. Chmiola, G. Yushin, Y. Gogotsi, C. Portet, P. Simon, Science 313 (2006) 1760–1763.
[30] C. Largeot, C. Portet, J. Chmiola, P.L. Taberna, Y. Gogotsi, P. Simon, Journal of American Chemical Society 130 (2008) 2730–2731.
[31] J. Chmiola, C. Largeot, P.L. Taberna, P. Simon, Y. Gogotsi, Angewandte Chemie International Edition 47 (2008) 3392–3395.
[32] H. Nishihara, H. Itoi, T. Kogure, P.X. Hou, H. Touhara, F. Okino, T. Kyotani, Chemistry –– A European Journal 15 (2009) 5355–5363.
[33] H. Nishihara, T. Kyotani, Advanced Materials 24 (2012) 4473–4498.
[34] H.Q. Li, J.Y. Luo, X.F. Zhou, C.Z. Yu, Y.Y. Xia, Journal of Electrochemical Society 154 (2007) A731–A736.
[35] D.W. Wang, F. Li, M. Liu, G.Q. Lu, H.M. Cheng, Journal of Physical Chemistry C 112 (2008) 9950–9955.
[36] Y. Liang, D. Wu, R. Fu, Langmuir 25 (2009) 7783–7785.
[37] G.W. Sun, J.T. Wang, X.J. Liu, D.H. Long, W.M. Qiao, L.H. Ling, Journal of Physical Chemistry C 114 (2010) 18,745–18,751.

[38] M.P. Tate, B.W. Eggiman, J.D. Kowalski, H.W. Hillhouse, Langmuir 21 (2005) 10,112–10,118.
[39] J. Jin, N. Nishiyama, Y. Egashira, K. Ueyama, Microporous and Mesoporous Materials 118 (2009) 218–223.
[40] K.S.W. Sing, D.H. Everett, R.A. Haul, L. Moscou, R.A. Pierotti, J. Rouquerol, T. Siemieniewska, Pure and Applied Chemistry 57 (1985) 603–619.
[41] R.P. Ball, R. Evans, Langmuir 5 (1989) 714–723.
[42] P.I. Ravikovitch, A.V. Neimark, Langmuir 18 (2002) 9830–9837.
[43] K. Morishige, N. Tateishi, Journal of Chemical Physics 119 (2003) 2301–2306.
[44] A. Grosman, C. Ortega, Langmuir 21 (2005) 10,515–10,521.
[45] J. Israelachvili, in: Intermolecular and Surface Forces, second ed., Academic Press, London, 1992.
[46] H.S. Zhou, S.M. Zhu, M. Hibino, I. Honma, Journal of Power Sources 122 (2003) 219–223.
[47] C. Vix-Guterl, E. Frackowiak, K. Jurewicz, M. Friebe, J. Parmentier, F. Béguin, Carbon 43 (2005) 1293–1302.
[48] A.B. Fuertes, G. Lota, T.A. Centeno, E. Frackowiak, Electrochimica Acta 50 (2005) 2799–2805.
[49] D.W. Wang, F. Li, H.T. Fang, M. Liu, G.Q. Lu, H.M. Cheng, Journal of Physical Chemistry B 110 (2006) 8570–8575.
[50] H.L. Lu, W.J. Dai, M.B. Zheng, N.W. Li, G.B. Ji, J.M. Cao, Journal of Power Sources 209 (2012) 243–250.
[51] R. Mysyk, E. Raymundo-Pinero, J. Pernak, F. Beguin, Journal of Physical Chemistry C 113 (2009) 13,443–13,449.
[52] W. Sugimoto, H. Iwata, K. Yokoshima, Y. Murakami, Y. Takasu, Journal of Physical Chemistry B 109 (2005) 7330–7338.
[53] M. Itagaki, S. Suzuki, I. Shitanda, K. Watanabe, Electrochemistry 75 (2007) 649–655.
[54] T.C. Wei, H.W. Hillhouse, Langmuir 23 (2007) 5689–5699.
[55] H. Probstle, C. Schmitt, J. Fricke, Journal of Power Sources 105 (2002) 189–194.
[56] L. Zheng, Y. Wang, X.W.X. Wang, H. An, L. Yi, Journal of Material Sciences 45 (2010) 6030–6037.